Global Fit to Inclusive Electron Scattering Data on Carbon and Oxygen in the Quasielastic, Resonance and Inelastic Continuum Regions

M. E. Christy,[1] A. Bodek,[2] and T.N. Gautam[3]

[1] *Thomas Jefferson National Accelerator Facility, Newport News, VA 23606, USA**
[2] *Department of Physics and Astronomy, University of Rochester, Rochester, NY 14627, USA*†
[3] *Hampton University, Hampton, Virginia 23668*

(Dated: August 29, 2023)

We report on an empirical fit to inclusive electron scattering cross sections for Carbon (and Oxygen) in the nuclear-elastic, nuclear-excitations, quasielastic, resonance and inelastic continuum regions. The fit describes all data (about 6600 ^{12}C and 250 ^{16}O differential cross section measurements) for all values of the square of the four-momentum transfer Q^2 down to $Q^2 = 0$ (including photoproduction). In the quasielastic (QE) region the fit is based on the super-scaling formalism with Rosenfelder Pauli suppression. In the QE region we extract parameterizations of a *multiplicative* "Longitudinal Quenching Factor" at low momentum $\mathbf{q}$ and an *additive* "Transverse Enhancement" contribution at intermediate $\mathbf{q}$. In the inelastic resonance and continuum region the fit is based on Fermi smeared free proton and neutron data. The fit is constrained by all existing world data as well as preliminary high precision cross section measurements from Jefferson Lab Hall C experiment E-04-001.

I. INTRODUCTION

A reliable parameterization of all inclusive electron scattering cross sections on nuclear targets has several applications in nuclear and particle physics. Examples include

1. Reliable evaluation of radiative corrections to measured electron scattering data.

2. Providing a benchmark for testing the validity of Monte Carlo generators for electron and neutrino scattering

3. Evaluation of background in electron scattering from polarized ammonia. In this case, the contributions from the unpolarized nitrogen relative to the polarized proton must be taken into account to extract spin dependent inclusive cross section asymmetries.

4. Measurement[1] of the Coulomb Sun Rule[2, 3] as a function of momentum transfer $\mathbf{q}$

The fit builds on an updated version of the 2012 Bosted-Mamyan fit[4, 5]. We incorporate additional measurements done after 2012, expand the validity of the fit to low values of momentum transfer, and include additional parameters (e.g. longitudinal quenching) not included in the original fit. In addition, we extract the Coulomb Sum Rule as a function of $\mathbf{q}$.

The fit includes the following components: (a) Nuclear-elastic scattering and excitation of nuclear states, (b) Quasielastic scattering and (c) Resonance production and the inelastic continuum. The parameterizations of the form factors for nuclear-elastic scattering and excitation of nuclear states are presented in [6]. A short description of the quasielastic and resonance production fits and the measurement of the Coulomb Sum Rule are presented in [1].

In this paper we present details of the empirical parameterizations of the quasielastic, resonance and inelastic continuum cross sections for ^{12}C and ^{16}O. (Extension of the fit to all nuclei are reported in a subsequent publication).

II. INCLUSIVE ELECTRON-NUCLEON SCATTERING

A. Description in terms of longitudinal and transverse virtual photon cross sections

In terms of the incident electron energy, E_0, the scattered electron energy, $E^{'}$, and the scattering angle, θ, the absolute value of the exchanged 4-momentum squared in electron-nucleon scattering is given by

$$Q^2 = (-q)^2 = 4E_0E^{'}\sin^2\frac{\theta}{2}, \tag{1}$$

the mass of the undetected hadronic system is

$$W^2 = M^2 + 2M\nu - Q^2, \tag{2}$$

and the square of the 3-momentum transfer $\mathbf{q}$ is

$$\mathbf{q}^2 = Q^2 + \nu^2 \tag{3}$$

Here M the average nucleon mass and $\nu = E_0 - E'$. In these expressions we have neglected the electron mass which is negligible for the kinematics studied.

In the one-photon-exchange approximation, the spin-averaged cross section for inclusive electron-proton scattering can be expressed in terms of the photon helicity

*Electronic address: christy@jlab.org
†Electronic address: bodek@pas.rochester.edu

coupling as

$$\frac{d\sigma}{d\Omega dE'} = \Gamma\left[\sigma_T(W^2,Q^2) + \epsilon\sigma_L(W^2,Q^2)\right], \quad (4)$$

where σ_T (σ_L) is the cross section for photo-absorption of purely transverse (longitudinal) polarized photons,

$$\Gamma = \frac{\alpha E^{'}(W^2 - M_N^2)}{(2\pi)^2 Q^2 M E_0(1-\epsilon)} \quad (5)$$

is the flux of virtual photons, $\alpha = 1/137$ is the fine structure constant, and

$$\epsilon = \left[1 + 2(1+\frac{\nu^2}{Q^2})\tan^2\frac{\theta}{2}\right]^{-1} \quad (6)$$

is the relative flux of longitudinal virtual photons (sometimes referred to as the virtual photon polarization). Since Γ and ϵ are purely kinematic factors, it is convenient to define the reduced cross section

$$\sigma_r = \frac{1}{\Gamma}\frac{d\sigma}{d\Omega dE'} = \sigma_T(W^2,Q^2) + \epsilon\sigma_L(W^2,Q^2). \quad (7)$$

All the hadronic structure information is therefore, contained in σ_T and σ_L, which are only dependent on W^2 and Q^2.

B. Description in terms of structure functions

Alternatively, the cross section can be written in terms of structure functions as follows

$$\begin{aligned}\frac{d\sigma}{d\Omega dE'} &= \sigma_M[\mathcal{W}_2(W^2,Q^2) + 2\tan^2(\theta/2)\mathcal{W}_1(W^2,Q^2)] \\ \sigma_M &= \frac{\alpha^2\cos^2(\theta/2)}{[2E\sin^2(\theta/2)]^2} = \frac{4\alpha^2 E'^2}{Q^4}\cos^2(\theta/2) \quad (8)\end{aligned}$$

where σ_M is the Mott cross section, $\alpha = 1/137$ is the fine structure constant. The $\mathcal{F}_1$ and $\mathcal{F}_2$ structure functions are related to $\mathcal{W}_1$ and $\mathcal{W}_2$ by $\mathcal{F}_1 = M\mathcal{W}_1$ and $\mathcal{F}_2 = \nu\mathcal{W}_2$. The structure functions are typically expressed as functions of Q^2 and W^2 (or alternatively ν or $x = Q^2/(2M\nu)$. The target mass scaling variable [7–9] is ξ_{TM} where,

$$\xi_{TM} = \frac{Q^2}{M\nu[1+\sqrt{1+Q^2/\nu^2}]}. \quad (9)$$

The quantity R is defined as the ratio σ_L/σ_T, and is related to the structure functions by,

$$R(x,Q^2) = \frac{\sigma_L}{\sigma_T} = \frac{\mathcal{F}_2}{2x\mathcal{F}_1}(1+\frac{4M^2x^2}{Q^2}) - 1 = \frac{\mathcal{F}_L}{2x\mathcal{F}_1}, \quad (10)$$

where $\mathcal{F}_L$ is called the longitudinal structure function. The structure functions are expressed in terms of σ_L and σ_T as follows:

$$\begin{aligned}K &= \frac{Q^2(1-x)}{2Mx} = \frac{2M\nu - Q^2}{2M} \quad (11)\\ \mathcal{F}_1 &= \frac{MK}{4\pi^2\alpha}\sigma_T \quad (12)\\ \mathcal{F}_2 &= \frac{\nu K(\sigma_L+\sigma_T)}{4\pi^2\alpha(1+\frac{Q^2}{4M^2x^2})} \quad (13)\\ \mathcal{F}_L(x,Q^2) &= \mathcal{F}_2\left(1+\frac{4M^2x^2}{Q^2}\right) - 2x\mathcal{F}_1, \quad (14)\end{aligned}$$

or

$$2x\mathcal{F}_1 = \mathcal{F}_2\left(1+\frac{4M^2x^2}{Q^2}\right) - \mathcal{F}_L(x,Q^2). \quad (15)$$

In addition, $2x\mathcal{F}_1$ is given by

$$2x\mathcal{F}_1(x,Q^2) = \mathcal{F}_2(x,Q^2)\frac{1+4M^2x^2/Q^2}{1+R(x,Q^2)}, \quad (16)$$

or equivalently

$$\mathcal{W}_1(x,Q^2) = \mathcal{W}_2(x,Q^2)\times\frac{1+\nu^2/Q^2}{1+R(x,Q^2)}. \quad (17)$$

C. Description in terms of response functions

As mentioned earlier parameterizations of the form factors for nuclear-elastic scattering and excitation of nuclear states are given in [6]. The following formalism is used in the extraction of forms factors from experimental cross sections on nuclear targets. The electron scattering differential cross section is written in terms of longitudinal ($\mathcal{R}_L(\mathbf{q},\nu)$) and transverse ($\mathcal{R}_T(\mathbf{q},\nu)$) nuclear response functions [32] which are typically extracted as a function of $\mathbf{q}$ (instead of Q^2). Since this formalism is used for the extraction of nuclear elastic form factor and form factors for the excitation of nuclear states, there is additional factor of Z^2 in the expression:

$$\frac{d\sigma}{d\nu d\Omega} = \sigma_M[A\mathcal{R}_L(\mathbf{q},\nu) + B\mathcal{R}_T(\mathbf{q},\nu)] \quad (18)$$

where σ_M is the Mott cross section, $A = (Q^2/\mathbf{q}^2)^2$ and $B = \tan^2(\theta/2) + Q^2/2\mathbf{q}^2$. For nuclear elastic scattering at very low $\mathbf{q}$ $Q^2 = \mathbf{q}^2$ to a good approximation.

The relationship between the nuclear response functions, and structure functions is

$$\begin{aligned}\mathcal{R}_T(\mathbf{q},\nu) &= \frac{2\mathcal{F}_1(\mathbf{q},\nu)}{M} \quad (19)\\ \mathcal{R}_L(\mathbf{q},\nu) &= \frac{\mathbf{q}^2}{Q^2}\frac{\mathcal{F}_L(\mathbf{q},\nu)}{2Mx} \quad (20)\end{aligned}$$

or

$$\begin{aligned}\mathcal{R}_T(\mathbf{q},\nu) &= \frac{\mathbf{q}^2}{Q^2}\frac{K}{2\pi^2\alpha}\sigma_T \quad (21)\\ \mathcal{R}_L(\mathbf{q},\nu) &= \frac{K}{4\pi^2\alpha}\sigma_L \quad (22)\end{aligned}$$

Data Set	Q^2_{Min} (GeV^2)	Q^2_{Max} (GeV^2)	# Data Points	Normalization	χ^2_{pdf}
Yamaguchi71 [10]					
Gomez74 [11, 12]					
Whitney [13]					
Barreau83 [14]					
O'Connell87 [15]					
Baran88 [16]					
Bagdasaryan88 [17]					
Sealock89 [18]					
Day93 [19]					
Dai19 [20]					
Arrington96[21]					
Arrington99 [22]					
Fomin10 [23, 24]					
Gaskell [25, 26]					
Ryan [27]					
E04-001 (Preliminary) [28–30]					
Zeller73 [31] (not used)					

TABLE I: A summary table of the ^{12}C data sets used in the universal fit. Shown are the number of data points, the Q^2 range of each set, the normalization factor, and the universal fit χ^2 per degree of freedom for each set. The Zeller73 [31] data set is inconsistent with all other data sets and is not used.

Where the units of $\mathcal{R}_L(\mathbf{q},\nu)$ and $\mathcal{R}_T(\mathbf{q},\nu)$ correspond to the units of M^{-1}.

. The square of the electric and magnetic form factors for elastic scattering and nuclear excitations are obtained by the integration of the measured response functions over ν for each nuclear state. When form factors for nuclear elastic scattering and nuclear excitations are extracted from electron scattering data there is an additional factor of Z^2 in the definition of σ_M (where Z is the atomic number of the nucleus) Figure 1 (taken from our previous publication[6]) illustrates the contribution of nuclear excitations to the scattering cross sections. Shown are experimental radiatively corrected inelastic electron scattering cross sections on ^{12}C for excitation energies less than 50 MeV. Also shown are the corresponding cross sections from our universal fit to all ^{12}C data. The cross sections for excitation energies less than 12 MeV are multiplied by (1/6). The three states below 10 MeV are purely longitudinal.

The pink solid line is the predicted total cross section from our universal fit described below. The QE contribution is shown as the dashed blue line and contribution of the "Transverse Enhancement/Meson Exchange Currents"($TE(\nu,Q^2)$) is shown as the dot-dashed line. Most of the cross section measurements are from Yamaguchi71[10]. The cross sections for E_o=54 MeV at 180^0 are from Goldemberg64[33] and the the cross sections for E_o=65 MeV at 180^0 are from deForest65[34]. The measurements at 180^0 are only sensitive to the transverse form factors.

III. FITS TO FREE PROTON AND NEUTRON DATA

At the start, we update previous parametrizations[35] of electric and magnetic elastic scattering form factors for free protons and free neutrons (extracted from deuteron data). In the updated fits we include all recent data on hydrogen and deuterium.

We also update previous parameterizations [36, 37] of σ_L and σ_T in the resonance and inelastic continuum regions for free protons and free neutrons. In the updated fits we include all recent data. We extract independent fits for the virtual photo-absorption cross sections for protons and neutrons. We do not constrain $R = \frac{\sigma_L}{\sigma_T}$ for protons and neutrons to be the same, as was done in previous fits to $R(\nu,Q^2)$[38].

IV. THE ^{12}C DATA SETS USED IN THE UNIVERSAL FIT

The ^{12}C data sets used in the universal fit are summarized in Table I. Shown are the number of data points, the Q^2 range of each set, the normalization factor extracted from the fit, and the universal fit χ^2 per degree of freedom for each set. The Zeller73 [31] data set is inconsistent with all other data sets and is not used.

V. COULOMB CORRECTIONS

In modeling QE and inelastic (pion production) scattering from bound nucleons, Coulomb corrections to QE and inelastic pion production processes are taken into account using the "Effective Momentum Approximation"(EMA) [39, 40]. The approximation is a simple energy gain/loss method, using a slightly higher incident and scattered electron energies at the vertex than

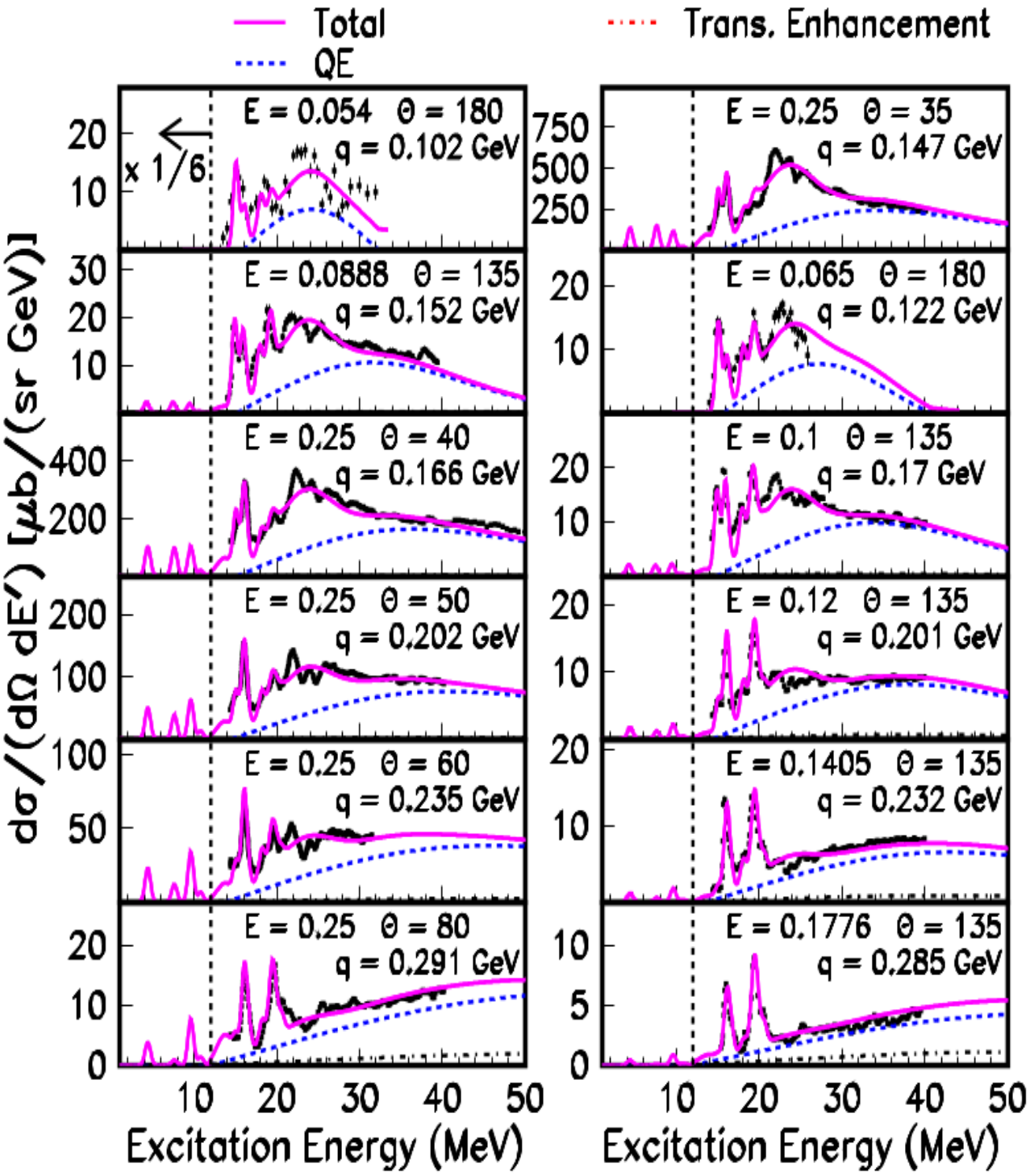

FIG. 1: Radiatively corrected inelastic electron scattering cross sections on ^{12}C for excitation energies less than 50 MeV. The cross sections for excitation energies less than 12 MeV are multiplied by (1/6). The pink solid line is the predicted total cross section from our universal fit to all electron scattering data on ^{12}C. The dashed blue line is the QE contribution and the "Transverse Enhancement/Meson Exchange Currents" contribution is the dot-dashed line. The data are from Yamaguchi71[10] except for the cross sections for E_o=54 MeV and 180^0 (from Goldemberg64[33]) and the cross sections for E_o=65 MeV and 180^0 (from deForest65[34]). The measurements at 180^0 are only sensitive to the transverse form factors.

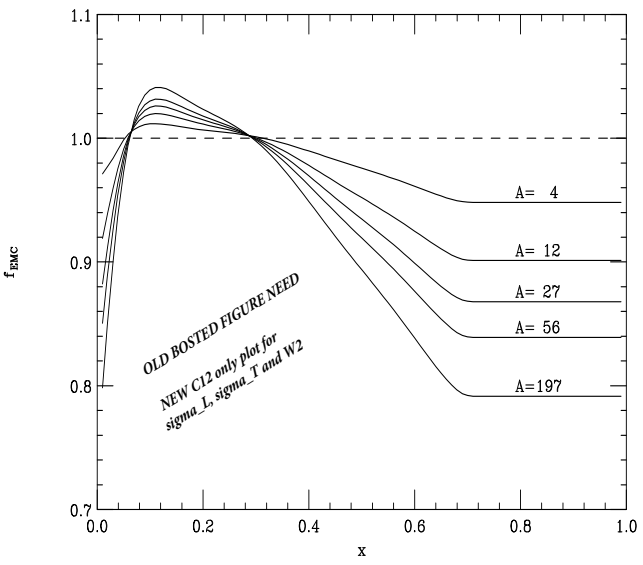

FIG. 2: Illustration of the ξ-dependence of the EMC ratios for C_L, C_T, and C_{W2} for σ_L, σ_T and $\mathcal{W}_2$, respectively. Note that these corrections are applied to the free proton and neutron data *before* Fermi smearing.

measured in the lab. The effective incident energy is $E_{eff} = E_0 + V_{eff}$, and the effective scattered energy is $E'_{eff} = E' + V_{eff}$.

Assuming a spherical charge distribution in the nucleus (of radius R) the electrostatic potential inside the charged sphere can be defined as followed:

$$V(r) = \frac{3\alpha(Z-1)}{2R} + \frac{\alpha(Z-1)}{2R}\frac{r}{R} \tag{23}$$

where R (in units of GeV) is given by:

$$R = 1.1A^{(1/3)} + 0.86A^{(-1/3)}. \tag{24}$$

$$\begin{aligned} V_{eff} &= 0.775V(r=0) \\ &= 0.775\ \frac{3}{2}\ \alpha(Z-1)/R \end{aligned} \tag{25}$$

where Z and A are the atomic number and atomic weight of the nucleus, respectively. This value for V_{eff} is consistent with value of $V_{eff} = 3.1 \pm 0.25$ extracted from a comparison of positron and electron QE scattering cross sections on carbon[40]. The effective Q^2_{eff} is given by

$$Q^2_{eff} = 4(E_0 + V_{eff})(E' + V_{eff})\sin^2(\theta/2) \tag{26}$$

The structure functions are calculated with $Q^2 = Q^2_{eff}$ and $E' = E'_{eff}$. In addition, there is a focusing factor $F_{foc} = \frac{E_0+V_{eff}}{E_0}$ which modifies the Mott cross section The modified Mott cross section is

$$\begin{aligned} \sigma_{M-eff} &= F_{foc}\frac{\alpha^2\cos^2(\theta/2)}{[2E_{eff}\sin^2(\theta/2)]^2} \\ &= \sigma_M\frac{E_0}{E_0+V_{eff}}. \end{aligned} \tag{27}$$

Parameters	C_L	C_T	C_{W2}
P_{13}			
P_{14}			
P_{15}			
P_{16}			
P_{17}			

TABLE II: Parameters of fitted parameters of the EMC ratios (corrections for bound nucleons) C_L, C_T, and C_{W2} for σ_L, σ_T and $\mathcal{W}_2$, respectively.

The differential cross section model (σ_{model}) is used to correct the measured cross sections σ_{meas} and yield a coulomb corrected(CC).

VI. RESONANCES AND INELASTIC CONTINUUM

To extract cross sections for electron scattering for bound nucleons in ^{12}C in the resonance and inelastic continuum regions we Fermi smear the free proton and neutron virtual photo-absorption cross sections $\sigma_L(W^2, Q^2)$ and $\sigma_L(W^2, Q^2)$ as follows:

$$\begin{aligned} \sigma^F_L(W^2,Q^2) &= C_L(x)\sum_i [Z\sigma^p_L((W'_i)^2,Q^2) \\ &+ (A-Z)\sigma^n_L((W'_i)^2,Q^2)]f_i \end{aligned} \tag{28}$$

$$\begin{aligned} \sigma^F_T(W^2,Q^2) &= C_T(x)\sum_i [Z\sigma^p_T((W'_i)^2,Q^2) \\ &+ (A-Z)\sigma^n_T((W'_i)^2,Q^2)]f_i \end{aligned} \tag{29}$$

Here, $\sigma^F_L(W^2, Q^2)$ and $\sigma^F_T(W^2, Q^2)$ are Fermi smeared cross sections for bound nucleons in ^{12}C. The shifted values $\mathcal{W}'_i$ are given by

$$\begin{aligned} (\mathcal{W}'_i)^2 &= W^2 + \xi_i k_F^{inelastic}\mathbf{q} - 2E^{inelastic}_{\rm shift}(\nu + M) \\ \xi_i &= -3 + 6(i-1)/98 \\ f_i &= 0.0245e^{(-\xi_i^2/2)}, \end{aligned} \tag{30}$$

The extracted value of $k_F^{inelastic}$ from the fit is 0.360 GeV.

The sum can be described as a step-wise integration over a Gaussian whose width is controlled by a Fermi momentum k_F, truncated at $\pm 3\sigma$, with a central shift in W related to the nucleon removal energy $E^{inelastic}_{\rm shift}(\mathbf{q})$ which is $\mathbf{q}$ dependent because of the optical potential[41, 42] of final state nucleons and pions in the nuclear field of the spectator A-1 nucleus. $E^{inelastic}_{\rm shift}(\mathbf{q})$ is extracted from the overall fit and is given by:

$$E^{inelastic}_{\rm shift}(\mathbf{q}) = NEED--EXPRESS \tag{31}$$

1. *Nuclear corrections to σ_L and σ_T for bound nucleons*

The $C_L(x)$ and $C_T(x)$ terms are EMC corrections (corrections to σ_L and σ_T for bound nucleons). These corrections (as a function of ξ) are extracted from the overall

fit.

$$C_(\xi) = 1 + P_{13}\xi + P_{14}\xi^2 + P_{15}\xi^3 + P_{16}\xi^4 + P_{17}\xi^5, \quad (32)$$

In terms of structure functions: C_{W1}=C_T and

$$C_{W2} = \frac{C_L\sigma_L + C_T\sigma_T}{\sigma_L + \sigma_T}$$

The fitted parameters are given in Table II Since $\sigma_L^F(W^2, Q^2)$ and $\sigma_L^F(W^2, Q^2)$ are fitted independently, the extracted values also yield $R^{C12} = \sigma_L^F/\sigma_T^F$ for ^{12}C.

Figure 2 Illustrates the ξ-dependence of the EMC ratios for C_L, C_T, and C_{W2} for σ_L, σ_T and $\mathcal{W}_2$, respectively. Note that these corrections are applied to the free proton and neutron data *before* Fermi smearing.

VII. QUASIELASTIC SCATTERING]

A. Superscaling

The theoretical description of the *QE longitudinal response* within the ψ' SuSA (Super Scaling Approximation) formalism[43–46] is in good agreement with experimental data at moderate Q^2. In this analysis we extend the application of the formalism to describe the longitudinal and transverse response functions at all values of Q^2 down to Q^2=0 by the addition of parameters accounting for a *multiplicative* QE "Quenching Factor" for the longitudinal response ($F^L_{quench}(\mathbf{q})$) at low $\mathbf{q}$, and parameters to describe an *additive* enhancement of the transverse response ($TE(\nu, Q^2)$) at intermediate $\mathbf{q}$

The ψ' superscaling variable is given by the following expression:

$$\psi' \equiv \frac{1}{\sqrt{\xi_F}} \frac{\lambda' - \tau'}{\sqrt{(1+\lambda')\tau' + \kappa\sqrt{\tau'(1+\tau')}}}, \quad (33)$$

where $\xi_F \equiv [\sqrt{1+\eta_F^2} - 1]$, $\eta_F \equiv K_F^{QE}/M_n$, $\lambda \equiv \nu/2M_n$, $\kappa \equiv |\mathbf{q}|/2M_n$ and $\tau \equiv |Q^2|/4M_n^2 = \kappa^2 - \lambda^2$.

The ψ' superscaling variable includes a correction that accounts for the removal energy from the nucleus. This is achieved by replacing ν with $\nu' = \nu - E^{QE}_{\rm shift}$, which forces the maximum of the QE response to occur at $\psi' = 0$. This is equivalent to taking $\lambda \to \lambda' = \lambda - \lambda_{\rm shift}$ with $\lambda_{\rm shift} = E^{QE}_{\rm shift}/2M_n$ and correspondingly $\tau \to \tau' = \kappa^2 - \lambda'^2$ in eq. (33).

Although we only fit cross section measurements on ^{12}C, it is expected within this model that QE scattering on all nuclei (except for the deuteron) is described using the same universal superscaling function, and the only parameters which are specific to each nucleus are the Fermi broadening parameter K_F^{QE} and the energy shift parameter $E^{QE}_{\rm shift}$. In our fit to the ^{12}C data we include $\mathbf{q}$ dependent $E^{QE}_{\rm shift}(\mathbf{q})$ parameter for the QE process to account for both the removal energy and the optical potential of final state nucleons[41]. $E^{QE}_{\rm shift}(\mathbf{q})$ for ^{12}C is constrained to be greater than 16 MeV, which is the separation energy of a proton from ^{12}C

$$\begin{aligned} E^{QE}_{\rm shift}(GeV) &= 0.020\ GeV \quad [\ \mathbf{q} > 1GeV\ ] \quad (34)\\ E^{QE}_{\rm shift}(GeV) &= 0.020 - 0.004\sqrt{1-\mathbf{q}} \quad [\ \mathbf{q} < 1GeV\ ] \end{aligned}$$

In our fit we allow $E^{QE}_{\rm shift}$ for QE scattering[41] to be different from $E^{inelastic}_{\rm shift}$ for pion production processes[42].

B. QE longitudinal scaling function

The QE longitudinal response function is given by:

$$\mathcal{R}_L^{QE}(\mathbf{q}, \nu) = \frac{FN(\psi')}{K_F^{QE}} \times G(Q^2, \nu), \quad (35)$$

where $FN(\psi')$ is the longitudinal scaling function and $G(Q^2, \nu)$ contains kinematic factors and form factors.

The longitudinal and transverse scaling functions in the Relativistic Fermi Gas (RFG) model[45] are the same and given by:

$$FN(\psi') = \frac{3}{4}(1 - \psi'^2)\theta(1 - \psi'^2). \quad (36)$$

A better ψ' superscaling function can be extracted from the longitudinal QE cross section at intermediate $Q^2 \approx 0.3$ GeV^2, where Pauli blocking is negligible the QE peak and Δ resonance are well separated from each other). We show results with three different superscaling functions. For purpose of comparison in ^{12}C, all functions set to zero for $\psi' < -3.0$ and for $|\psi'| > \psi'_{max}$ and are normalized to 1.0. For ^{12}C the nominal Fermi broadening parameter is K_F^{QE}=0.228 GeV for ^{12}C.. The superscaling functions $FN(\psi')$ are fitted using the following functional form:

$$\begin{aligned} FN(\psi') &= \frac{P_1 \times h(\psi')}{[1 + P_2^2(\psi' + P_3)^2](1 + e^{P4\psi'})} \\ &\quad \text{for} -2.2 < \psi' < 5.0 \quad (37) \end{aligned}$$

where in general $h(\psi')$ =1.0. In our fit we make sure that the functions goes smoothly to zero at $\psi' = 5.0$ by using:

$$h(\psi') = (1 - |\psi'|/5.0)^2 \times (1 + |\psi'|/5.0)^2$$

The parameters for the three different models are given in Table I.

Fig. 3 shows: (a) the longitudinal scaling function $FN(\psi')$ for the RFG model (solid blue line), (b) from a 2005 fit by Amaro et. al. [44] (dashed black line), (c) from a 2020 fit to the QE data by Amaro et. al. [45] (solid red line), and (d) from our 2023 fit to ^{12}C data only (solid green line).

At $\mathbf{q}$=0 the longitudinal cross section for all inelastic processes (including QE) must be zero. Therefore, the multiplicative $\mathbf{q}$ dependent QE "Quenching Factor " $F^L_{quench}(\mathbf{q})$ is zero for $\mathbf{q}$=0 and 1.0 at high $\mathbf{q}$.

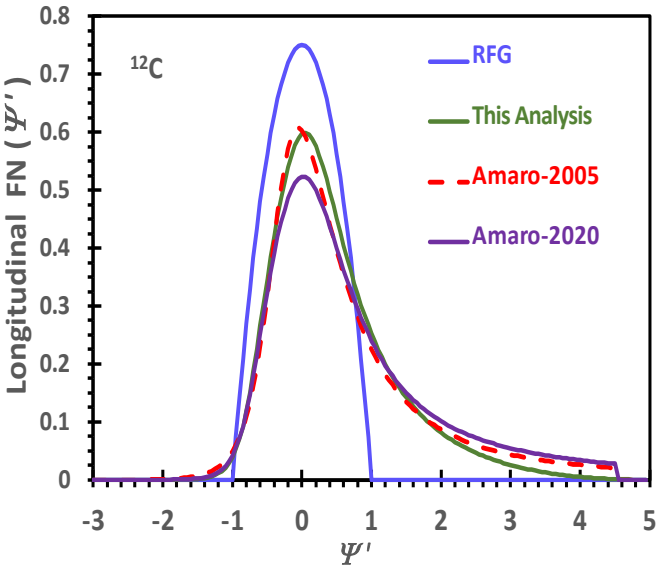

FIG. 3: Longitudinal scaling function $FN(\psi')$ for the RFG model (solid blue line); $FN(\psi')$ from a 2005 fit by Amaro et. al. [44] (dashed black line), from a 2020 fit to the QE data by Amaro et. al. [45] (solid red line), and from our 2023 fit to ^{12}C data only (solid green line).

Parameters	Amaro 2020	Amaro 2005	This-analysis 2023
$\mathbf{h}(\psi')$	1.0	1.0	$(1-\lvert\psi'\rvert/5.0)^2\times$ $(1+\lvert\psi'\rvert/5.0)^2$
$\mathbf{P_1}$	2.8377	1.33370	3.780
$\mathbf{P_2}$	1.9438	1.71190	2.078
$\mathbf{P_3}$	0.6731	0.19525	0.7081
$\mathbf{P_4}$	−3.8538	−1.69000	−4.1604
$\psi'_{\mathbf{max}}$	4.5	4. 5	5.0
$E^{QE}_{\rm shift}$	0.02 GeV	0.02 GeV	0.016-0.020 GeV $*$

TABLE III: Parameters for $FN(\psi')$ shown of Fig.3. These include (1) the 2005 fit by Amaro et. al. [44], (2) the 2020 fit by Amaro et. al.[45] and (3) our 2023 fit to ^{12}C data only. Here $K_F^{QE} = 0.228$ GeV. $*$ see equation 34.

C. QE Transverse scaling function

In the SuSA model the longitudinal and transverse scaling functions are the same. Experimentally, the transverse scaling function does not scale (i.e. it depends on $\mathbf{Q^2}$) and is larger than the longitudinal scaling function. This has been referred to as "Transverse Enhancement". In most Monte Carlo (MC) generators the single nucleon longitudinal and transverse QE scaling functions are the same. In addition, some generators include a transverse Meson Exchange Currents contribution (from 2-body currents) which yield two nucleons in the final state. This contribution populates the region between the QE peak and pion production. However, there is also a contribution to transverse response function form the interference of 1-body and 2-body currents which yields a single nucleon in the final state. This contribution from interference enhances the cross section in the region of the QE peak[47, 48].

In summary, the overall enhancement of the transverse response function originates from several sources.

- The transverse scaling function is larger than the longitudinal scaling function (as expected in relativistic mean field (RMF) calculations)[47, 49]
- Two body (2b) Meson Exchange Currents (MEC) which yield two nucleons in the final state.
- Interference between the one body (1b) and two body currents increases the transverse response in the region of the QE peak and yields a single nucleon in the final state
- Two body isobar excitations which increase the transverse response.

D. Pauli suppression

The average Pauli blocking factor for the RFG model is given by the following expression[50, 51]:

$$\begin{aligned}\langle F^{RFG}_{Pauli}(\mathbf{q})\rangle &= \frac{3}{4}x - \frac{1}{16}x^3 \quad (for\ \mathbf{q} < 2K_F^{QE}) \\ &= 1 \qquad\qquad\quad (for\ \mathbf{q} > 2K_F^{QE}),\end{aligned} \tag{38}$$

where we use $K_F^{QE} = 0.228$ GeV for ^{12}C. However, the average Pauli suppression for the RFG model is larger than the Pauli suppression for more realistic nucleon momentum distributions.

In this analysis we use Rosenfelder method[45, 46, 52] which is a simple way to account for Pauli suppression *in any model of the QE distribution.*

As an example, the method is illustrated on the top panel of Fig. 4 for the RFG model with K_F^{QE}=0.228 GeV, $E^{QE}_{\rm shift}$= 16 MeV and $\mathbf{q}$=0.3 GeV. $FN(\nu,\mathbf{q})$ is the superscaling function $FN(\psi',\mathbf{q})$ for RFG, which is normalized to 1.0 in the absence of Pauli suppression.

The Pauli suppressed $FN_{Pauli}(\psi',\mathbf{q})$ distribution for the RFG model is shown versus ν as the solid blue line labeled *"RFG-Pauli suppressed"*. For $\nu < E^{QE}_{\rm shift}$, the Pauli suppressed distribution $FN_{Pauli}(\nu,\mathbf{q})$ distribution is zero. For $\nu > E^{QE}_{\rm shift}$ It is determined as follows:

$$FN_{Pauli}(\nu,\mathbf{q}) = FN_{positive}(\nu,\mathbf{q}) - FN_{negative}(\nu,\mathbf{q}).$$

$FN_{positive}(\nu,\mathbf{q})$ (solid green line labeled *RFG-pos*) is the superscaling distribution $FN(\psi',\mathbf{q})$ calculated with $\nu' = +[\nu - E^{QE}_{\rm shift}]$.

$FN_{negative}(\nu,\mathbf{q})$ (solid red line labeled *"RFG-neg"*) is $FN(\psi',\mathbf{q})$ calculated with $\nu' = -[\nu - E^{QE}_{\rm shift}]$.

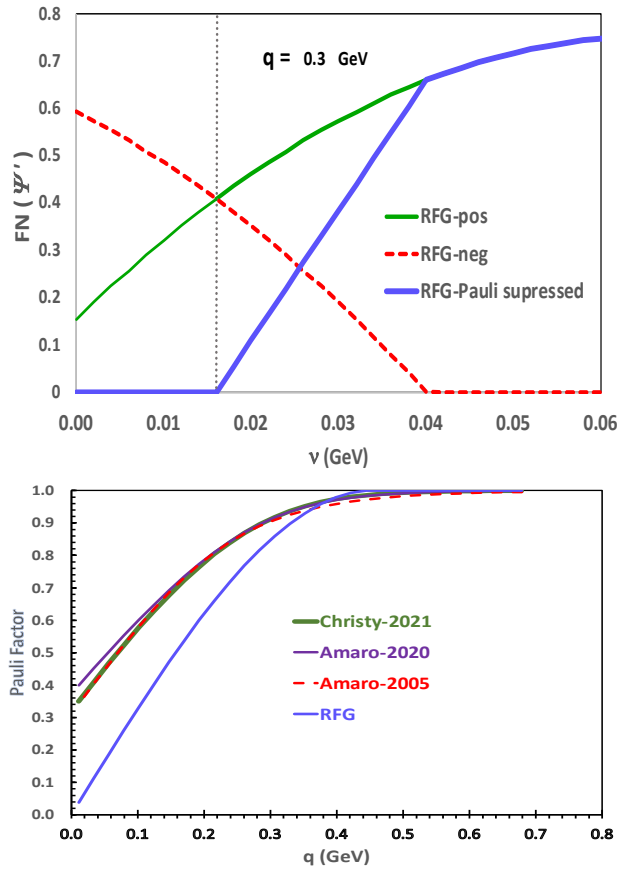

FIG. 4: **Top panel**: The general procedure for the determination of Pauli suppression is illustrated for the RFG distribution as an example. The solid blue line is the Pauli suppressed RFG $FN_{Pauli}(\nu,\mathbf{q})$ distribution for K_F^{QE}=0.228 GeV, $E_{\rm shift}^{QE}$= 16 MeV and $\mathbf{q}$=0.3 GeV. See text for details. **Bottom panel**:]The average integrated Pauli suppression for the superscaling functions shown in Fig. 3): $\langle F_{Pauli}^{Amaro20}(\mathbf{q})\rangle$, $\langle F_{Pauli}^{Amaro05}(\mathbf{q})\rangle$, $\langle F_{Pauli}^{This\ analysis}(\mathbf{q})\rangle$ and RFG model $\langle F_{Pauli}^{RFG}(\mathbf{q})\rangle$.

E. Excitation energy

The relation between the energy transfer ν and the excitation energy of the nucleus $E_x(Q^2)$ is

$$E_x = \nu - \frac{Q^2}{2M_{nucleus}} \tag{39}$$

At low Q^2 the energy transfer ν and the excitation energy E_x are the same. In the Rosenfelder method the Pauli factor is zero for $\nu < E_{\rm shift}^{QE}(\mathbf{q})$. Consequently, by requiring the $\mathbf{q}$ dependent $E_{\rm shift}^{QE}(\mathbf{q})$ to be above the separation energy E_s of a proton from the nucleus (16 MeV for ^{12}C and 12 MeV for ^{16}O) ensures that the Pauli factor is zero for excitation energies (E_x) smaller than the separation energy E_s.

However, at larger Q^2 the can be non-zero in the following region"

$$E_s - \frac{Q^2}{2M_{nucleus}} < Ex < E_s \tag{40}$$

Therefore, we multiply the Pauli factor by the following correction factor $G(Q^2,\nu)$ to insure that the product is zero at $E_x = E_s$. Here

$$G(Q^2,\nu) = ???? \tag{41}$$

F. Average Pauli suppression integrated over ν

The integral of the superscaling function $F_N(\psi')$ over the region $-3.0 < \psi' < 5.0$ is equal to 1.0. The average Pauli suppression $\langle F_{Pauli}(\mathbf{q})\rangle$ is equal to the value of the Pauli suppressed $FN_{Pauli}(\mathbf{q},\nu)$ distribution integrated over ν with $\nu > E_{\rm shift}^{QE}$. It is also equal to the Pauli suppressed $FN_{Pauli}(\psi')$ integrated over ψ' where $\psi'_{min} = \psi'(\nu'=0)$ or $\psi'_{min} = \psi'(\lambda'=0)$. Therefore, the average Pauli suppression factor $\langle F_{Pauli}(\mathbf{q})\rangle$ is:

$$\begin{aligned}\langle F_{Pauli}(\mathbf{q})\rangle &= 1 - 2\int_{-3.0}^{\psi'_{min}} FN(\psi')d\psi' \\ \psi'_{min} &= \frac{1}{\sqrt{\xi_F}}\frac{-\tau'_{min}}{\sqrt{(\tau'_{min}+\kappa\sqrt{\tau'_{min}(1+\tau'_{min})}}}\end{aligned} \tag{42}$$

where for λ'=0, $\tau'_{min}(\lambda'=0) = \kappa^2$ and $\kappa \equiv |\mathbf{q}|/2M_n$.

The bottom panel of Fig. 4 shows the average integrated Pauli suppression for the RFG model $\langle F_{Pauli}^{RFG}(\mathbf{q})\rangle$, and for the three superscaling function parameters given in Table IV (and shown in Fig. 3).

The average Pauli suppression $\langle F_{Pauli}(\mathbf{q})\rangle$ for the four models is independent of $E_{\rm shift}$, but depends on the parameter $\mathbf{q}$ (or $x = \mathbf{q}/K_F^{QE}$) as shown in Fig. 4.

G. Parameterization of the average integrated Pauli suppression

The Pauli suppression factor for $x > 3.0$ is 1.0. For $x < 3.0$ we parametrize the average integrated Pauli suppression factor for the three superscaling models by the following function:

$$\langle F_{Pauli}^{model}(x)\rangle = \sum_{j=0}^{j=3} k_j (x)^j \tag{43}$$

The parameters for the three superscaling models are given in Table IV.

VIII. DETAILS OF THE ANALYSIS

A. Rosenbluth separation of $\mathcal{R}_T^{QE}$ and $\mathcal{R}_L^{QE}$

As mentioned above, in modeling the QE response we use the same scaling function for both $\mathcal{R}_L^{QE}(\mathbf{q},\nu)$

Parameters	Amaro 2020 $x < 3.0$	Amaro 2005 $x < 3.0$	This-analysis 2021 $x < 3.0$
K_F^{QE}	0.228	0.228	0.228
$\mathbf{k_o}$	0.3505	0.2897	0.2975
$\mathbf{k_1}$	0.6806	0.7988	0.7612
$\mathbf{k_2}$	−0.2315	−0.3070	−0.2687
$\mathbf{k_3}$	0.0253	0.0397	0.0307

TABLE IV: Parameters of fits (equation 43) describing the average integrated Pauli suppression for the three superscaling functions with $FN(\psi')$ shown in Fig. 3).

and $\mathcal{R}_T^{QE}(\mathbf{q},\nu)$ and fit for empirical corrections to the response functions. For $\mathcal{R}_T^{QE}$ we extract an *additive* "Transverse Enhancement/MEC" contribution (which includes both single nucleon and two nucleon final states). As shown in [53] "Transverse Enhancement" increases $\mathcal{R}_T^{QE}$ with the largest fractional contribution around Q^2=0.3 GeV^2. For $\mathcal{R}_L^{QE}$ we extract a *multiplicative* $\mathbf{q}$ dependent "Longitudinal Quenching Factor", $F_{quench}(\mathbf{q})$, which decreases $\mathcal{R}_L^{QE}$ at low $\mathbf{q}$.

Since $\frac{d^2\sigma}{d\Omega d\nu}$ measurements span a large range of θ and $\mathbf{q}$, parametrizations of both the "Transverse Enhancement" and the longitudinal QE quenching factor $F^L_{quench}(\mathbf{q})$ can be extracted from the fit.

B. The 2012 Bosted-Mamyan fit

Because our analysis builds on the 2012 fit by Bosted and Mamyan [4, 5] we present a brief summary of that fit. The primary purpose of the 2012 Bosted-Mamyan fit was to model Born level electron scattering cross sections to be used in calculations of radiative corrections to electron measurements on nuclear targets.

The fit was made to all electron scattering data for nuclei with $A > 2$. The fit is based on previous empirical fits to electron-proton and electron-neutron scattering, and takes into account the effects of Fermi motion plus a substantial "Transverse Enhancement" contribution that increases the peak cross section and also fills in the dip between the quasi-elastic peak and the $\Delta(1232)$ resonance. Briefly the Bosted-Mamyan fit includes the following:

1. All electron scattering data for nuclei with $A > 2$.
2. Coulomb corrections[39, 40] using the Effective Momentum Approximation (EMA) in modeling scattering from nuclear targets.
3. Nuclear elastic form factors.
4. Free nucleon elastic form factors[35].
5. A fixed value of $E^{QE}_{\rm shift}$=0.020 GeV for ^{12}C.
6. $FN(\psi')$ from Amaro-2005[44] to model QE scattering (not including Pauli suppression).
7. Fit parameters for a $\mathbf{q}$ and ν dependent "Transverse Enhancement/MEC" model.
8. Gaussian Fermi smeared free nucleon resonance and inelastic structure functions (using previous fits to inelastic electron scattering data on hydrogen[36] and deuterium[37]).
9. Photo-production data in the resonance region and inelastic continuum.
10. Unpublished parametrization of the EMC effect (nuclear dependence of Deep Inelastic Scattering) by S. Rock in 1994.
11. For QE scattering the fit is valid for $Q^2 > 0.2$ GeV^2. Below Q^2 of 0.2 GeV^2 the fit is not reliable since it uses the RFG model *average* Pauli factor $\langle F^{RFG}_{Pauli}(\mathbf{q})\rangle$ (given in equation 38) to approximate the effect of Pauli blocking and any other low $\mathbf{q}$ suppression of the QE cross section.

C. Updated fit

The 2023 updated fit builds on the 2012 Bosted-Mamyan fit. In the fits reported here we only include data on ^{12}C. An analysis that includes data for a large range of nuclei[55, 56] will be reported in a subsequent publication.

A brief summary of the updates and improvements to the Bosted-Mamyan fit is given below:

1. All available electron scattering data on hydrogen, deuterium and ^{12}C. We include QE data at *all values* of Q^2 down to Q^2=0.01 GeV^2 ($\mathbf{q}$=0.1 GeV) (which were not included in the 2012 fit). In addition, we include additional data that was taken after 2012.
2. Coulomb corrections[39, 40] using the Effective Momentum approximation (EMA) in modeling scattering from nuclear targets are the same.
3. Updated ^{12}C nuclear elastic form factor and form factors for nuclear excitations[6](nuclear excitations were not included in the 2012 fit)
4. Updated parameters of the superscaling function $FN(\psi')$ including the Fermi broadening parameter K_F^{QE}.
5. Free nucleon elastic form factors[35] are re-derived from all available deuterium and hydrogen data[57].
6. Rosenfelder Pauli suppression[45, 46, 52] which reduces and changes the shape of the QE distribution at low ν and low $\mathbf{q}$ (these were not included in the 2012 fit).

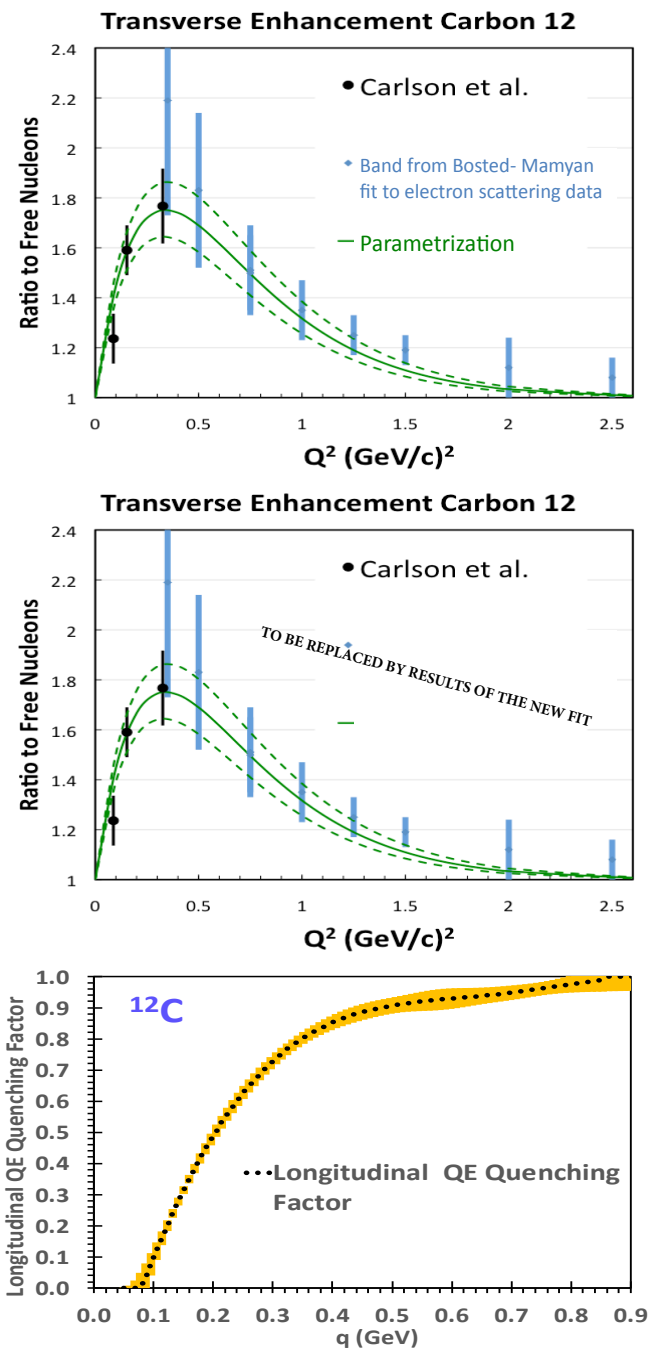

FIG. 5: **Top panel**: The "Transverse Enhancement/MEC" ratio ($\mathcal{R}_{TE}$) as a function of Q^2 from a *previous analysis* [53] done with the 2012 Bosted-Mamyan fit. Here, $\mathcal{R}_{TE}$ is ratio of the integrated (over W^2) transverse response function for QE electron scattering on nucleons bound in carbon (including transverse enhancement) divided by the integrated transverse response function for independent nucleons. The black points are extracted from Carlson *et al*[54], and the blue bands are extracted from the Bosted-Mamyan fit[5]. **Middle panel**: The $\mathcal{R}_{TE}$ ratio extracted from our updated 2023 fit. **Bottom panel**: QE "Longitudinal Quenching Factor" F^L_{quench} extracted from the electron scattering data on ^{12}C (dotted-black line with yellow error band).

7. A $\mathbf{q}$ dependent $E^{QE}_{\rm shift}(\mathbf{q})$ and $E^{inelastic}_{\rm shift}(\mathbf{q})$ parameters to account for both the nucleon removal energy and the optical potential[41] of final state nucleons and pions. (a fixed number was used in the 2012 fit).

8. Updates of the 2012 fits[36, 37] to proton and neutron inelastic electron scattering data[24] (in the nucleon resonance region and inelastic pion production continuum) (to be presented in a subsequent publication)

9. Photo-production data in the nucleon resonance region and inelastic pion production continuum.

10. Gaussian Fermi smeared nucleon resonance and inelastic pion production [36]. The Fermi broadening parameters for inelastic pion production and QE Fermi broadening parameters are not constrained to be the same,

11. New parametrizations of the medium modifications of both the transverse and longitudinal structure functions responsible for the EMC effect (nuclear dependence of inelastic scattering). This is applied to the free nucleon structure functions prior to application of the Fermi smearing

12. Parameters of an improved *additive* "Transverse Enhancement/MEC" contribution ($\mathcal{F}_1^{TE}(W^2,Q^2)$) to $\mathcal{F}_1$ for ^{12}C as described below.

13. Parameters to account for multiplicative low $\mathbf{q}$ quenching of the QE longitudinal response function (these were not included in the 2012 fit).

D. Additive "Transverse Enhancement/MEC"

The extracted *additive* transverse enhancement structure function $\mathcal{F}_1^{TE}(W^2,Q^2)$ combines the contributions from all sources. It is parameterized as two distorted Gaussians with Q^2 dependent widths and amplitudes. One is centered around $W \approx 0.88$ GeV (for single nucleons in the final state) and the other at $W \approx 1.2$ GeV (for two nucleons in the final state). We set $\mathcal{F}_1^{TE}$=0 for $\nu < \nu_{min}$ (ν_{min}=16.5 MeV which is the removal energy of a proton from ^{12}C). For $\nu > \nu_{min}$ $\mathcal{F}_1^{TE}$ is given by:

$$\begin{aligned}
\mathcal{F}_1^{TE} &= max((f_1^A + f_1^B), 0.0) \qquad (44)\\
f_1^A &= a_1 Y \cdot [(W^2 - W^2_{min})^{1.5} \cdot e^{-(W^2-b_1)^2/2c_1^2}]\\
f_1^B &= a_2 Y \cdot (Q^2 + q_o^2)^{1.5} \cdot [e^{-(W^2-b_2)^2/2c_2^2}]\\
Y &= Ae^{-Q^4/12.715} \frac{(Q^2+q_0^2))}{(0.13380+Q^2)^{6.90679}}\\
a_1 &= 0.091648,\ a_2 = 0.10223\\
W^2_{min} &= M_p^2 + 2M_p\nu_{min} - Q^2
\end{aligned}$$

where Q^2 is in units of GeV^2, M_p is the proton mass, A is the atomic weight, $q_0^2 = 1.0\times10^{-4}$, $b_1 = 0.77023$, $c_1 =$

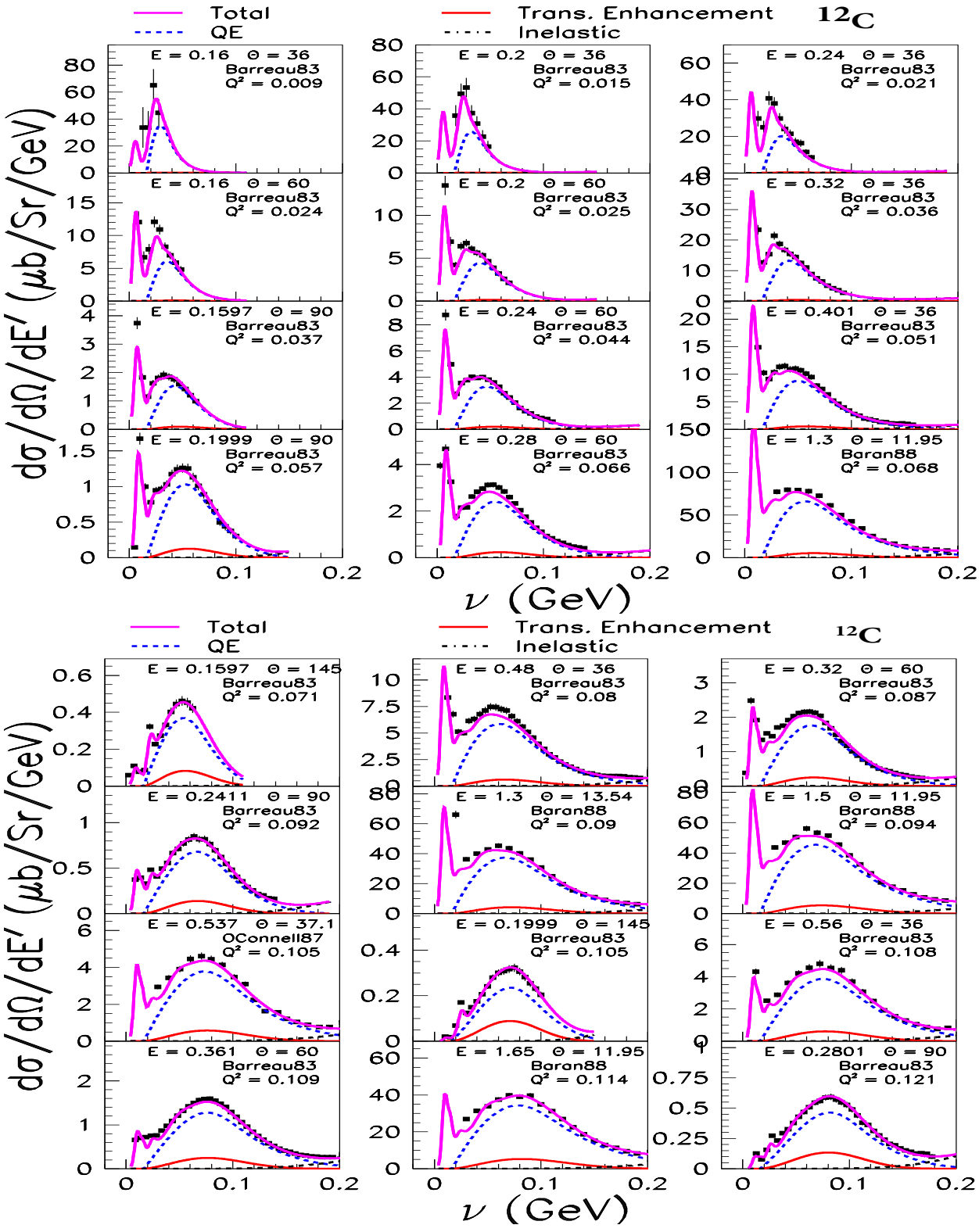

FIG. 6: Comparisons our fit to a subset of electron scattering differential cross section data with $Q^2 < 0.12$ GeV^2. The total $\frac{d^2\sigma}{d\nu d\Omega}$ is shown as the solid purple line. The dashed blue line is the QE differential cross section. The TE contribution to the QE differential cross section is shown as the solid red line. Inelastic pion production processes are shown as the dot-dashed black line. The fit is in good agreement with the cross section data for both small and large angles. The values of Q^2 increase from top bottom from Q^2=0.009 to Q^2=0.121 GeV^2. Data are from Barreau 1983[14] and Baran 1988[16].

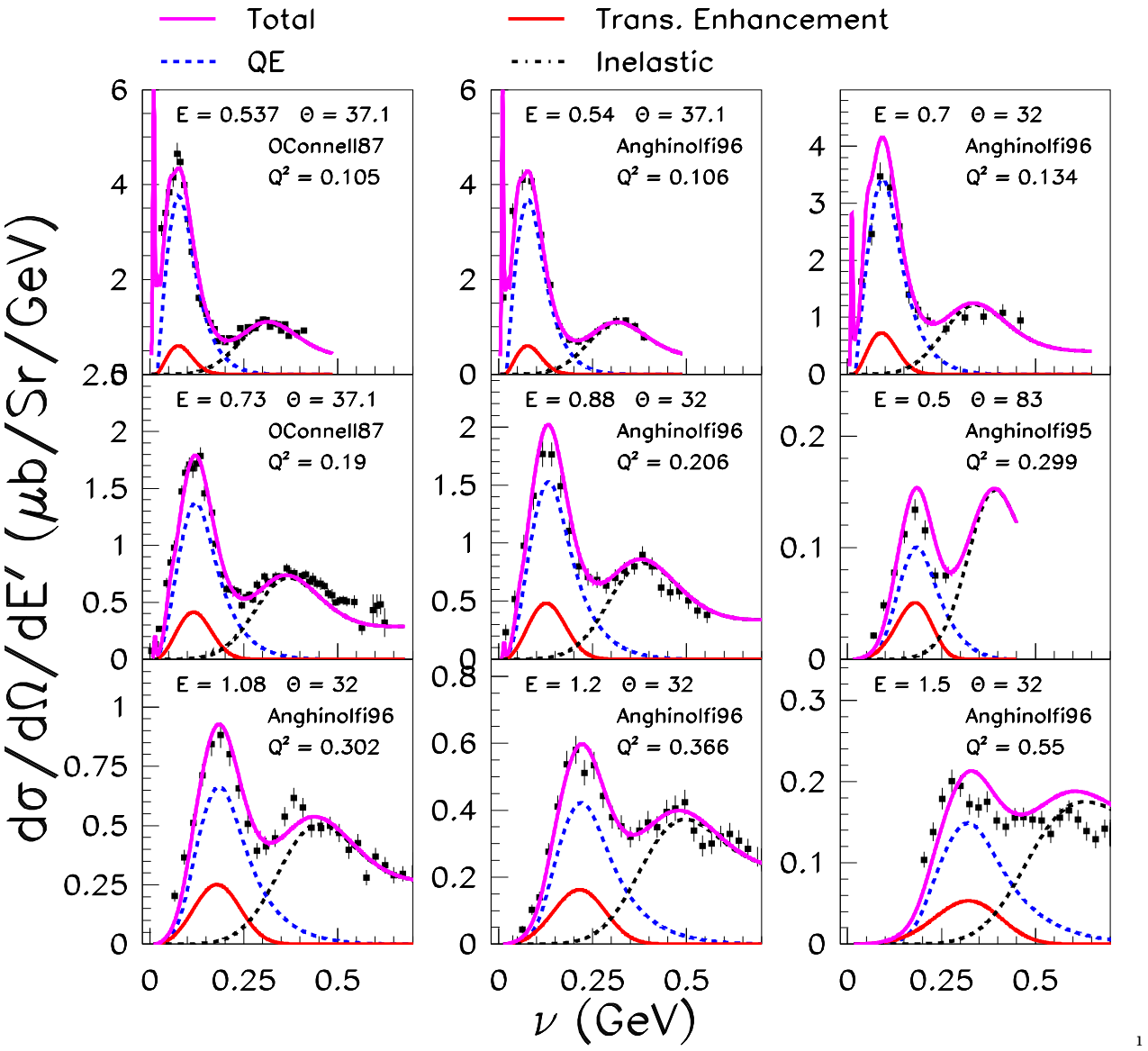

FIG. 7: Comparison of our fit (using ^{12}C parameters) to all available $\frac{d^2\sigma}{d\nu d\Omega}$ measurements on ^{16}O.

$0.077051+0.26795Q^2$, b_2= 1.275, and c_2= 0.375. The parameters of the empirical model of $\mathcal{F}_1^{TE}(W^2, Q^2)$ in electron scattering can be used to predict the $\mathcal{F}_1^{TE}(W^2, Q^2)$ contribution in neutrino scattering[58, 59].

The top panel of Figure 5 we show the "Transverse Enhancement/MEC" ratio ($\mathcal{R}_{TE}$) as a function of Q^2 from a *previous analysis*[53] done with the 2012 Bosted-Mamyan fit. Here, $\mathcal{R}_{TE}$ is ratio of the integrated (over W^2) transverse response function for QE electron scattering on nucleons bound in carbon (including transverse enhancement) divided by the integrated transverse response function for independent nucleons. The black points are extracted from Carlson *et al*[54], and the blue bands are extracted from the 2012 Bosted-Mamyan fit[5]). The Middle panel of Figure 5 shows the $\mathcal{R}_{TE}$ ratio extracted from our updated 2023 fit.

E. Multiplicative "Longitudinal Quenching Factor"

At low values of **q** there is overlap in ν between the QE contribution and the contribution of nuclear excitations. Although nuclear excitations are included in the model, we exclude QE differential cross section data with excitation energy below 35 MeV from the fit. However, when we compare to experimental data we show the fit and data at all values of ν.

The "quenching" of R_L^{QE} (in addition to the expected suppression from Pauli blocking) extracted from the data within the framework of our superscaling model is described by the following multiplicative factor:

$F^L_{quench}(\mathbf{q})$ is unity for x>3.75, and is zero for x<0.35. For $0.35 < x < 4.0$ it is parameterized by:

$$F^L_{quench}(\mathbf{q}) = \frac{(x-0.2)^2}{(x-0.18)^2}\big[1.0 + A_1(3.75-x)^{1.5} + A_2(3.75-x)^{2.5} + A_3(3.75-x)^{3.5}\big] \quad (45)$$

where $x = \mathbf{q}/K_F^{QE}$. A_1=−0.13152 A_2=0.11693, and A_3=−0.03675.

The bottom panel of Fig. 5 shows $F^L_{quench}(\mathbf{q})$ for ^{12}C extracted from the fit. The yellow band corresponds to the statistical error from the fit, with a systematic error of 0.02 (added in quadrature) to account for the choice of parametrization function.

If another formalism is used to model QE scattering (e.g. RFG or spectral functions) then the quenching factor for the model $F^{L-model}_{quench}(\mathbf{q})$ is given by:

$$F^{L-model}_{quench}(\mathbf{q}) = \frac{\langle F^{This-analysis}_{Pauli}(\mathbf{q})\rangle}{\langle F^{model}_{Pauli}(\mathbf{q})\rangle} F^L_{quench}(\mathbf{q}) \quad (46)$$

The total (from all sources) longitudinal QE suppression factor extracted from the data is the product of two terms.

$$F^{This-analysis}_{QE-total}(x) = \langle F^{This-analysis}_{Pauli}(x)\rangle \times F^L_{quench}(x)$$

where $\langle F^{This-analysis}_{Pauli}(x)\rangle$ is the average Pauli blocking factor of the QE cross section integrated over ν (calculated using our superscaling function).

IX. COMPARISON OF THE FIT TO CROSS SECTION MEASUREMENTS ON ^{12}C AND ^{16}O

Comparisons of our fit to a subset of electron scattering differential cross section data with $Q^2 < 0.12$ GeV^2 are shown in Fig. 6. The total (differential) cross section is shown as the solid purple line. The dashed blue line is the QE differential cross section. The TE contribution to the QE differential cross section is shown as the solid red line. Inelastic pion production processes are shown as the dot-dashed black line. The fit is in good agreement with the cross section data for both small and large angles. The values of Q^2 increase from top bottom from Q^2=0.009 to Q^2=0.121 GeV^2. A large fraction of the electron scattering data are available on the electron scattering archive[55, 56]. The lowest $\mathbf{q}$ data are from references [14–16, 18].

There is not enough QE data for ^{16}O to perform a complete analysis. We find that the QE fit parameters for ^{12}C also describe all available data on ^{16}O. Comparison of our fit (using ^{12}C parameters) to all available $\frac{d^2\sigma}{d\nu d\Omega}$ measurements on ^{16}O is shown in Fig. 7. Data are from O'Connell 1987[15], Anghinolfi 1995 [62] and Anghinolfi 1996[63].

X. LONGITUDINAL AND TRANSVERSE RESPONSE FUNCTIONS FOR ^{12}C

Comparisons of the fit to electron scattering $\frac{d^2\sigma}{d\Omega d\nu}$ measurements[14, 16, 55, 56] at different values of θ for $\mathbf{q}$ values close to 0.30, 0.38 and 0.57 GeV (corresponding to extractions of R_L and R_T by Jourdan[60, 61]) are shown in Fig. 8. Shown are the total $\frac{d^2\sigma}{d\Omega d\nu}$ cross section (solid-purple line), the total minus the contribution of nuclear excitations (solid-blue), the QE cross section without TE (dashed-blue), the TE contribution (solid-red), and inelastic pion production (dot-dashed black). An estimated resolution smearing of 3.5 MeV has been applied to the excitations to better match the data. The fit is in good agreement with all electron scattering data for both small and large θ.

A comparison between our extraction of $\mathcal{R}_L(\mathbf{q},\nu)$ and $\mathcal{R}_T(\mathbf{q},\nu)$ and the extraction (for only three values of $\mathbf{q}$) by Jourdan[60, 61] are shown in Fig. 9. At the lowest $\mathbf{q}$ our $\mathcal{R}_L(\mathbf{q},\nu)$ is a somewhat lower and our $\mathcal{R}_T(\mathbf{q},\nu)$ is a somewhat higher. (The Jourdan analysis includes data from only two experiments). Also shown are two 1-body+2-body current (1b+2b) calculations: First Principle Green's Function Monte Carlo" (GFMC)[47] and "Energy Dependent-Relativistic Mean Field" (ED-RMF)[48]. In our fit, we show each nuclear excitation with excitation energy E_x at $\nu = E_x + \mathbf{q}^2/2M_{C12}$ where M_{C12} is the mass of the carbon nucleus.

In contrast, the ED-RMF calculations group all excitations in two fixed ν peaks as shown in Fig.9, and the GFMC calculations do not show any nuclear excitations. Both calculations are in reasonable agreement with our analysis in the QE region. In both models there is enhancement of $\mathcal{R}^{QE}_T(\mathbf{q},\nu)$ if only 1b currents are included and additional enhancement if both 1b and 2b currents are included. The curves labeled 2b in Fig. 9 show the enhancement in $\mathcal{R}^{QE}_T(\mathbf{q},\nu)$ from 2b currents only [i.e. (1b+2b) minus (1b only)], while our empirical extraction of $TE(\mathbf{q},\nu)$ shown in Fig. 9 models the enhancement in $\mathcal{R}_T(\mathbf{q},\nu)$ from all sources.

XI. DISCUSSION

To illustrate the main features of the fit, the response function F_2 is plotted versus W in Fig. 10. The top curve in each plot is the sum of the there components: a quasi-elastic peak centered on M, a smaller broader "Transverse Enhancement" contribution, and the inelastic continuum. The Q^2 dependence of F_1 for ^{12}C is illustrated in Figure. 11. Note the very prominent quasi-elastic and $\Delta(1231)$ peaks at low Q^2, which "disappear" rapidly at higher Q^2. The fit is compared with all world data for ^{12}C in Figure 12 where the ratios between fit and world data for ^{12}C are shown in six Q^2 bins as a function of W. Figure 13 shows the frequency distribution of the deviations (in percent) between data and fit for all the

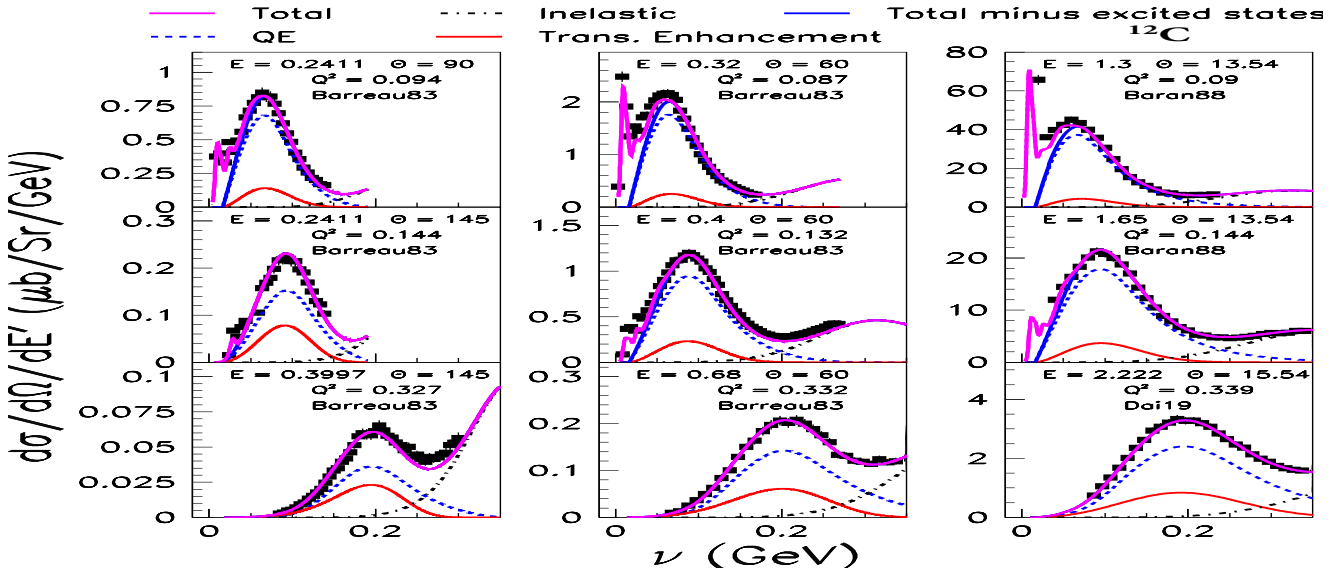

FIG. 8: Comparison of the fit to electron scattering $\frac{d^2\sigma}{d\Omega d\nu}$ measurements[14, 16, 55, 56] at $\mathbf{q}$ values close to 0.30, 0.38 and 0.57 GeV (and different scattering angles). Shown are total $\frac{d^2\sigma}{d\Omega d\nu}$ (solid-purple line), total minus the contribution of the nuclear excitations (solid-blue), the QE cross section without Transverse Enhancement (TE) (dashed-blue), the TE contribution (solid-red) and inelastic pion production (dot-dashed black line).

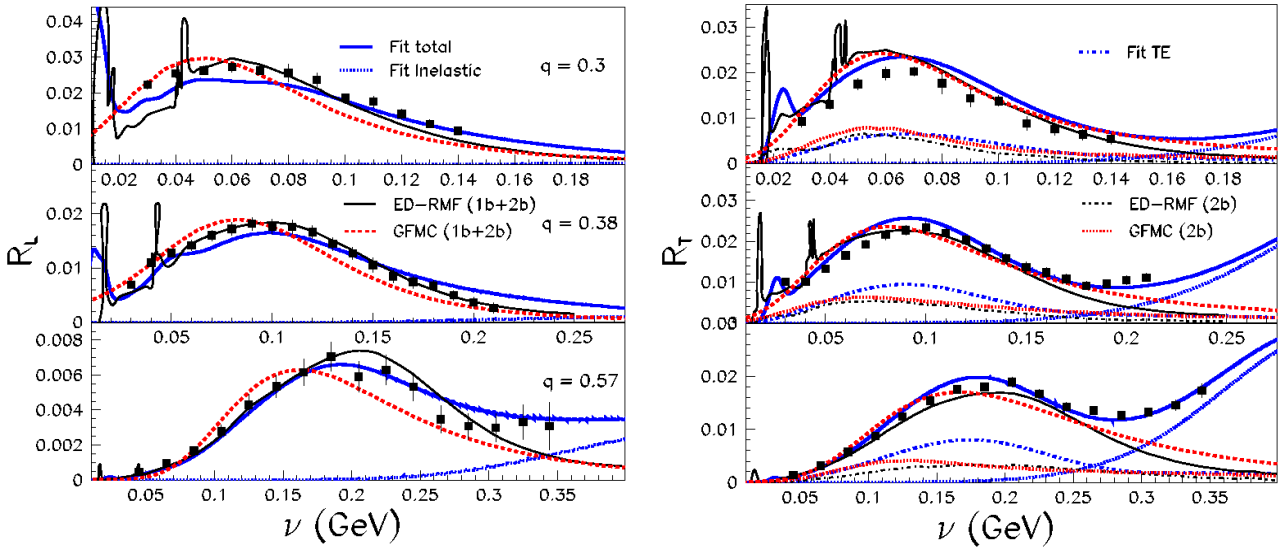

FIG. 9: Comparisons between our extraction of $\mathcal{R}_L(\mathbf{q},\nu)$ and $\mathcal{R}_T(\mathbf{q},\nu)$ and the extraction (for only three values of $\mathbf{q}$) by Jourdan[60, 61]. (The Jourdan analysis includes data from only two experiments). Also shown are comparisons to 1b+2b GFMC[47] and ED-RMF[48] theoretical predictions. In these two models the curves labeled 2b are the only contribution of 2-body currents to $TE(\mathbf{q},\nu)$. The transverse enhancement in both 1b and 2b currents is included in the total.

data points used.

XII. SUMMARY

We provide a universal fit to all inclusive electron scattering cross sections on ^{12}C. The fit can be used for a reliable evaluation of radiative corrections to measured electron scattering data and provides a benchmark for testing the validity of Monte Carlo generators for electron and neutrino scattering. The extraction of the Coulomb Sum Rule from the fit is discussed in the Appendix.

The 2023 Chirsty-Bodek-Gautam code is available at Where ??????????

A. acknowledgments

Research supported in part by the U.S. Department of Energy under University of Rochester grant number DE-SC0008475, and the Office of Science, Office of Nuclear Physics under contract DE-AC05-06OR23177.

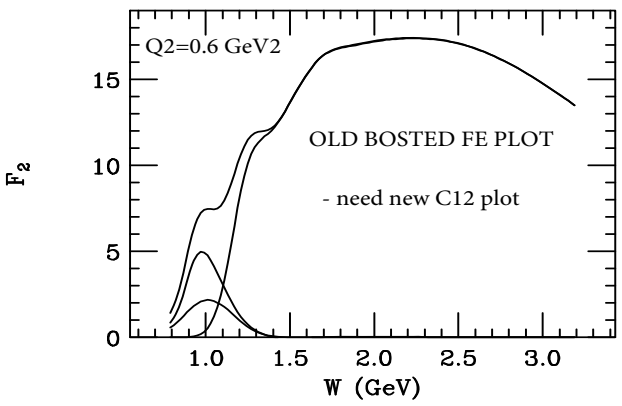

FIG. 10: Illustration of the W-dependence of the structure function $F_2(W, Q^2)$ for ^{12}C for $Q^2 = 0.6$ GeV^2. The upper curves are the sum of the three lower curves (quasi-elastic, "Transverse Enhancement", and inelastic, from left to right).

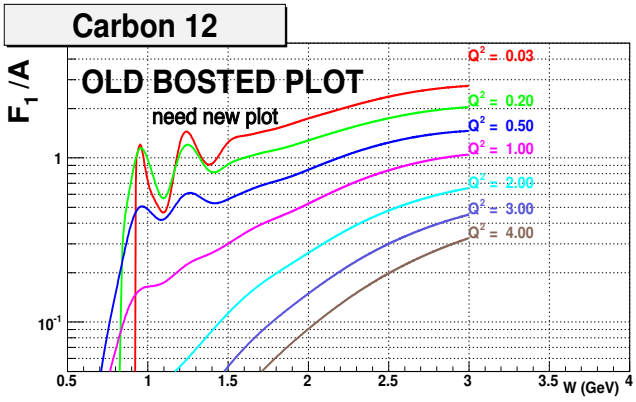

FIG. 11: Illustration of the W-dependence of the structure function $F_1(W, Q^2)$ (per nucleon) for ^{12}C for a wide range of Q^2 values (units are GeV^2).

Appendix A THE COULOMB SUM RULE

The inelastic Coulomb Sum Rule is the integral of $R_L(\mathbf{q}, \nu)d\nu$, *excluding the elastic peak and pion production processes*. It has contributions from QE scattering and from electro-excitations of nuclear states:

$$\mathrm{CSR}(\mathbf{q}) = \int R_L(\mathbf{q}, \nu)d\nu \quad (47)$$

$$= \int R_L^{QE}(\mathbf{q}, \nu)d\nu + G_E'^2(Q^2) \times Z^2 \sum_{all}^{L} F_i^2(\mathbf{q})$$

$$= G_E'^2(Q^2) \times \left[Z \int V_L^{QE}(\mathbf{q}, \nu)d\nu + Z^2 \sum_{all}^{L} F_i^2(\mathbf{q})\right].$$

We define $V^{QE}(\mathbf{q}, \nu)$ as the reduced longitudinal QE response, which integrates to unity in the absence of any suppression (e.g. Pauli blocking). The charge form factors for the electro-excitation of nuclear states $F_{iC}^2(\mathbf{q})$ is $G_{Ep}^2(Q^2) \times F_i^2(\mathbf{q})$. In order to account for the small contribution of the neutron and relativistic effects $G_E'^2(Q^2)$ is given by[32]:

$$G_E'^2(Q^2) = [G_{Ep}^2(Q^2) + \frac{N}{Z} G_{En}^2(Q^2)] \frac{1+\tau}{1+2\tau}, \quad (48)$$

where, G_{Ep} and G_{En} are the electric form factors of the proton and neutron respectively and $\tau = Q^2/4M_p^2$.

By dividing Eq. 47 by $ZG_E'^2(Q^2)$ we obtain the normalized inelastic Coulomb Sum Rule $SL(\mathbf{q})$:

$$SL(\mathbf{q}) = \int V_L^{QE}(\mathbf{q}, \nu)d\nu + Z \sum_{all}^{L} F_i^2(\mathbf{q}). \quad (49)$$

At high $\mathbf{q}$ it is expected that $S_L \to 1$ because both nuclear excitation form factors and Pauli suppression are small. At small $\mathbf{q}$ it is expected that $S_L \to 0$ because the all form factors for inelastic processes (QE and nuclear excitations) must be zero at $\mathbf{q}$=0.

Our universal fit provides the best measurement of QE Coulomb Sum Rule $SL(\mathbf{q})$ for several reasons. The measurement of $SL(\mathbf{q})$ requires the following: (a) Reliable extraction of both the longitudinal and transverse response functions as a function of $\mathbf{q}$ and ν. (b) Measurements of the contribution of nuclear excitations at small ν. (c) Estimation of the separate contributions of the QE and inelastic pion production to the longitudinal response function at high $\mathbf{q}$ and large ν.

Our universal fit addresses all of the above requirements. (a) By including all available electron scattering data on ^{12}C for a wide range of energy and angle, we have the most reliable extraction of the longitudinal and transverse response functions.(b) By parameterizing the form factors for all nuclear excitations in ^{12}C and ^{16}O we have a reliable measurement of the contribution of all nuclear excitations to $SL(\mathbf{q})$. (c) We extract the shape of the QE superscaling function at lower $\mathbf{q}$ where the contribution of pion production processes is small, and use it to estimate the QE contribution at larger $\mathbf{q}$ where the contribution of pion production processes is large.

Fig. 14 shows the various contributions to the extracted $S_L(\mathbf{q})$ for ^{12}C (dotted blue line with yellow error band). Shown are the QE contribution with only Pauli suppression (dotted-purple), the QE contribution suppressed by both "Pauli Suppression" and the longitudinal quenching factor $F_{quench}^L(\mathbf{q})$ labeled as QE suppressed (Pauli+Quench) (solid-green), and the contribution of nuclear excitations (red dashed line).

The left panel of Fig. 15 shows a comparison of the extracted $S_L(\mathbf{q})$ for ^{12}C (dotted-blue curve with yellow error band) to theoretical calculations. These include the Lovato 2016[47] "First Principle Green's Function Monte Carlo" (GFMC) calculation (solid-purple line), the Mihaila 2000[64] Coupled-Clusters based calculation (AV18+UIX potential, dashed-green), and the Cloet 2016[65] Random Phase Approximation (RPA) calculation (RPA solid-red). Our measurement for ^{12}C are in disagreement with Cloet 2016 RPA, and in reasonable

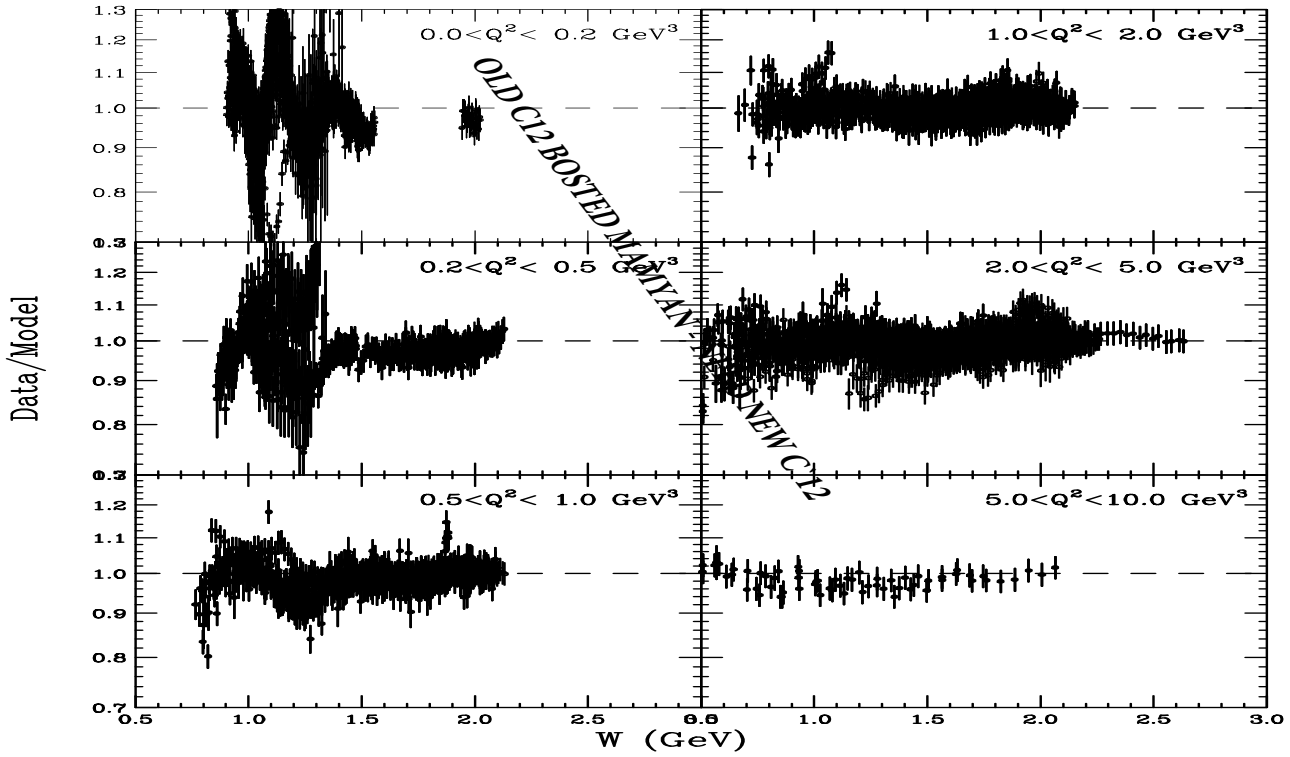

FIG. 12: Ratios between fit and world data for ^{12}C in six Q^2 bins as a function of W.

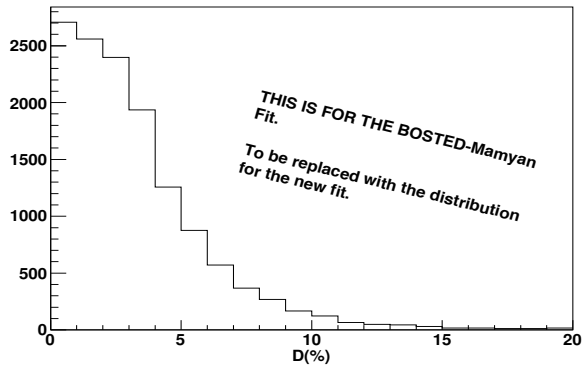

FIG. 13: Frequency distribution of deviations between data and fit (in percent) .

agreement with Lovato 2016 except near $\mathbf{q} \approx 0.30$ GeV where the contribution from nuclear excitations is significant.

The right panel of Fig. 15 shows $S_L(\mathbf{q})$ for ^{16}O (dotted-blue with green error band) compared to theoretical calculations. These include the Sobczyk 2020[66] "Coupled-Cluster with Singles-and Doubles (CCSD) NNLO$_{sat}$" (red-dashed line), and the Mihaila 2000[64] Coupled-Cluster calculation with (AV18+UIX potential, dashed green line). The data are in reasonable agreement with Sobczyk 2020.

[1] A. Bodek and M. E. Christy, Phys. Rev. C **106**, L061305 (2022), arXiv:2208.14772 [hep-ph] .

[2] D. Drechsel and M. M. Giannini, Rept. Prog. Phys. **52**, 1083 (1989).

[3] T. De Forest, Jr. and J. D. Walecka, Adv. Phys. **15**, 1 (1966).

[4] P. E. Bosted and V. Mamyan, "Empirical Fit to electron-nucleus scattering," (2012), arXiv:1203.2262 [nucl-th] .

[5] V. Mamyan, "Measurements of F_2 and R=σ_L/σ_T on Nuclear Targets in the Nucleon Resonance Region," (2012), phD thesis, University of Virginia (2010), arXiv:1202.1457 [nucl-ex] .

[6] A. Bodek and M. E. Christy, "Contribution of Nuclear Excitation Electromagnetic Form Factors in ^{12}C and ^{16}O to the Coulomb Sum Rule. arXiv: 2301.05650[nucl-th]," (2023), arXiv:2301.05650 [nucl-th] .

[7] O. Nachtmann, Nucl. Phys. B **63**, 237 (1973).

[8] H. Georgi and H. D. Politzer, Phys. Rev. D **14**, 1829 (1976).

[9] R. Barbieri, J. R. Ellis, M. K. Gaillard, and G. G. Ross,

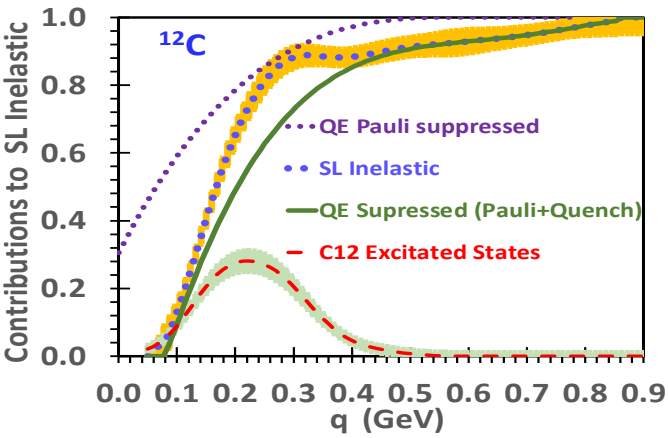

FIG. 14: The various contributions to $S_L(\mathbf{q})$ for ^{12}C (dotted blue with yellow error band) including: QE with Pauli suppression only (dotted-purple), QE suppressed by both "Pauli" and "Longitudinal Quenching" (solid-green), and the contribution of nuclear excitations (red-dashed with green error band)

Nucl. Phys. B **117**, 50 (1976).

[10] A. Yamaguchi, T. Terasawa, K. Nakahara, and Y. Torizuka, Phys. Rev. C **3**, 1750 (1971).

[11] J. Gomez *et al.*, Phys. Rev. D **49**, 4348 (1994).

[12] "Resonance Data Archive at Jefferson Lab Hall C," Https://hallcweb.jlab.org/resdata/.

[13] R. R. Whitney, I. Sick, J. R. Ficenec, R. D. Kephart, and W. P. Trower, Phys. Rev. **C9**, 2230 (1974).

[14] P. Barreau *et al.*, Nucl. Phys. **A402**, 515 (1983).

[15] J. S. O'Connell *et al.*, Phys. Rev. **C35**, 1063 (1987).

[16] D. T. Baran *et al.*, Phys. Rev. Lett. **61**, 400 (1988).

[17] D. S. Bagdasaryan *et al.*, "Measurement of the spectra of (e,e') scattering ^{9}Be and ^{12}C nuclei in the inelastic region at q^2 approximately 0.4 (gev/c)^2," (1988), yERPHI-1077-40-88.

[18] R. M. Sealock *et al.*, Phys. Rev. Lett. **62**, 1350 (1989).

[19] D. B. Day *et al.*, Phys. Rev. **C48**, 1849 (1993).

[20] M. Murphy *et al.*, Phys. Rev. C **100**, 054606 (2019), arXiv:1908.01802 [hep-ex] .

[21] J. Arrington *et al.*, Phys. Rev. **C53**, 2248 (1996), nucl-ex/9504003 .

[22] J. Arrington *et al.*, Phys. Rev. Lett. **82**, 2056 (1999), nucl-ex/9811008 .

[23] N. Fomin *et al.*, Phys. Rev. Lett. **105**, 212502 (2010), arXiv:1008.2713 [nucl-ex] .

[24] Y. Liang *et al.* (Jefferson Lab Hall C E94-110), Phys. Rev. C **105**, 065205 (2022), arXiv:nucl-ex/0410027 .

[25] J. Arrington *et al.*, Phys. Rev. C **104**, 065203 (2021), arXiv:2110.08399 [nucl-ex] .

[26] J. Seely *et al.*, Phys. Rev. Lett. **103**, 202301 (2009), arXiv:0904.4448 [nucl-ex] .

[27] P. J. Ryan, J. B. Flanz, R. S. Hicks, B. Parker, and G. A. Peterson, Phys. Rev. C **29**, 655 (1984).

[28] S. Alsalmi *et al.*, "Experimental investigation of the structure functions of ^{12}c in the resonance region," (2023), to be published.

[29] I. Albayrak *et al.*, "Precise measurements of electron scattering quasielastic cross sections on ^{12}c," (2023), to be published.

[30] S. A. Alsalmi, *Measurement of the Nuclear Dependence of F_2 and R=Sigma_L/Sigma_T in The Nucleon Resonance Region*, Ph.D. thesis, Kent State University, Kent State U. (2019).

[31] D. Zeller, *Investigation of the structure of the C-12 nucleus by high-energy electron scattering (DESY-F23-73-2)*, Master's thesis, University of Karlsruhe (1973).

[32] J. A. Caballero, M. C. Martinez, J. L. Herraiz, and J. M. Udias, Phys. Lett. B **688**, 250 (2010), arXiv:0912.4356 [nucl-th] .

[33] J. Goldemberg and W. C. Barber, Phys. Rev. **134**, B963 (1964).

[34] T. Deforest, J. Walecka, G. Vanpraet, and W. Barber, Physics Letters **16**, 311 (1965).

[35] P. E. Bosted, Phys. Rev. C **51**, 409 (1995).

[36] M. E. Christy and P. E. Bosted, Phys. Rev. C **81**, 055213 (2010), arXiv:0712.3731 [hep-ph] .

[37] P. E. Bosted and M. E. Christy, Phys. Rev. C **77**, 065206 (2008), arXiv:0711.0159 [hep-ph] .

[38] L. W. Whitlow, S. Rock, A. Bodek, E. M. Riordan, and S. Dasu, Phys. Lett. B **250**, 193 (1990).

[39] A. Aste, C. von Arx, and D. Trautmann, Eur. Phys. J. A **26**, 167 (2005), arXiv:nucl-th/0502074 .

[40] P. Gueye *et al.*, Phys. Rev. C **60**, 044308 (1999).

[41] A. Bodek and T. Cai, Eur. Phys. J. C **79**, 293 (2019), arXiv:1801.07975 [nucl-th] .

[42] A. Bodek and T. Cai, Eur. Phys. J. C **80**, 655 (2020), arXiv:2004.00087 [hep-ph] .

[43] C. Maieron, T. W. Donnelly, and I. Sick, Phys. Rev. C **65**, 025502 (2002), arXiv:nucl-th/0109032 .

[44] J. E. Amaro, M. B. Barbaro, J. A. Caballero, T. W. Donnelly, A. Molinari, and I. Sick, Phys. Rev. C **71**, 015501 (2005), arXiv:nucl-th/0409078 .

[45] J. E. Amaro, M. B. Barbaro, J. Caballero, R. González-Jiménez, G. D. Megias, and I. Ruiz Simo, J. Phys. G **47**, 124001 (2020), arXiv:1912.10612 [nucl-th] .

[46] G. D. Megias, M. V. Ivanov, R. Gonzalez-Jimenez, M. B. Barbaro, J. Caballero, T. W. Donnelly, and J. M. Udias, Phys. Rev. D **89**, 093002 (2014), [Erratum: Phys.Rev.D 91, 039903 (2015)], arXiv:1402.1611 [nucl-th] .

[47] A. Lovato, S. Gandolfi, J. Carlson, S. C. Pieper, and R. Schiavilla, Phys. Rev. Lett. **117**, 082501 (2016), arXiv:1605.00248 [nucl-th] .

[48] T. Franco-Munoz, R. González-Jiménez, and J. M. Udias, "Effects of two-body currents in the one-particle one-hole electromagnetic responses within a relativistic mean-field model," (2022), arXiv:2203.09996 [nucl-th] .

[49] G. D. Megías Vázquez, *Charged-current neutrino interactions with nucleons and nuclei at intermediate energies*, Ph.D. thesis, Seville U. (2017).

[50] Y.-S. Tsai, Rev. Mod. Phys. **46**, 815 (1974), [Erratum: Rev.Mod.Phys. 49, 421–423 (1977)].

[51] A. Bodek, "Pauli Blocking for a Relativistic Fermi Gas in Quasielastic Lepton Nucleus Scattering]," (2021), arXiv:2111.03631 [nucl-th] .

[52] R. Rosenfelder, Annals Phys. **128**, 188 (1980).

[53] A. Bodek, H. S. Budd, and M. E. Christy, Eur. Phys. J. C **71**, 1726 (2011), arXiv:1106.0340 [hep-ph] .

[54] J. Carlson, J. Jourdan, R. Schiavilla, and I. Sick, Phys. Rev. C **65**, 024002 (2002), arXiv:nucl-th/0106047 .

[55] O. Benhar, D. Day, and I. Sick, Rev. Mod. Phys. **80**, 189 (2008), arXiv:nucl-ex/0603029 .

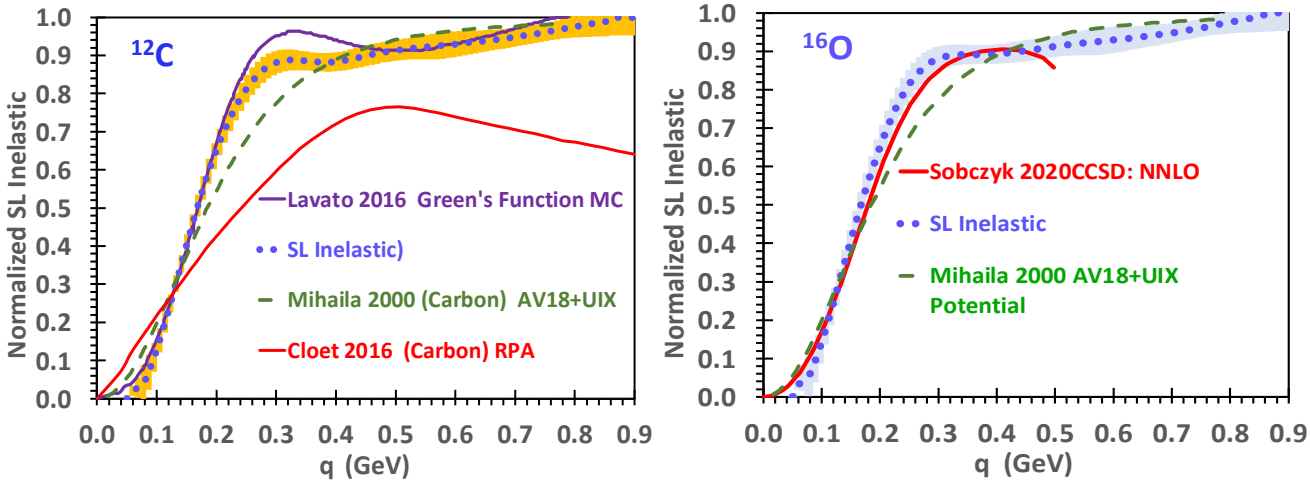

FIG. 15: **Left panel**: $S_L(\mathbf{q})$ for ^{12}C (dotted-blue with yellow error band) compared to theoretical calculations including Lovato 2016 GFMC [47] (solid-purple), (Mihaila 2000[64] (dashed-green), and RPA Cloet 2016[65] (solid-red). **Right panel**: $S_L(\mathbf{q})$ for ^{16}O (dotted-black with green error band) compared to theoretical calculations of Sobczyk 2020[66] (red-dashed) and Mihaila 2000 (dotted-dashed).

[56] D. Day, "Quasielastic Electron Nucleus Scattering Archives," (2004), e-Print: 2004.00087.

[57] M. E. Christy *et al.*, Phys. Rev. Lett. **128**, 102002 (2022), arXiv:2103.01842 [nucl-ex] .

[58] K. Gallmeister, U. Mosel, and J. Weil, Phys. Rev. C **94**, 035502 (2016), arXiv:1605.09391 [nucl-th] .

[59] S. Dolan, U. Mosel, K. Gallmeister, L. Pickering, and S. Bolognesi, Phys. Rev. C **98**, 045502 (2018), arXiv:1804.09488 [hep-ex] .

[60] J. Jourdan, Nucl. Phys. A **603**, 117 (1996).

[61] J. Jourdan, Phys. Lett. B **353**, 189 (1995).

[62] M. Anghinolfi *et al.*, J. Phys. G **21**, L9 (1995).

[63] M. Anghinolfi *et al.*, Nucl. Phys. A **602**, 405 (1996), arXiv:nucl-th/9603001 .

[64] B. Mihaila and J. Heisenberg, Phys. Rev. Lett. **84**, 1403 (2000), arXiv:nucl-th/9910007 .

[65] I. C. Cloët, W. Bentz, and A. W. Thomas, Phys. Rev. Lett. **116**, 032701 (2016), arXiv:1506.05875 [nucl-th] .

[66] J. E. Sobczyk, B. Acharya, S. Bacca, and G. Hagen, Phys. Rev. C **102**, 064312 (2020), arXiv:2009.01761 [nucl-th] .